MATERIALS SCIENCE

Efficient deep-blue luminescence based on dual-channel intra/intermolecular exciplexes

Zhen Zhang[1]†, Dehai Dou[1]†, Rongrong Xia[1], Peng Wu[1], Eduard Spuling[2], Ke Wang[1], Jin Cao[1], Bin Wei[1], Xifeng Li[1], Jianhua Zhang[1]*, Stefan Bräse[2,3]*, Zixing Wang[1]*

Highly efficient and stable blue organic light-emitting diodes (OLEDs) cannot be easily obtained simultaneously. In particular, the efficiency roll-off as a reference index to evaluate the lifetime of deep-blue OLED at high luminescence is still severe. A novel molecule (CzSiTrz) connected with carbazole and triazine fragments by a nonconjugated silicon atom is designed. An intramolecular charge transfer emission and intermolecular exciplex luminescence in the aggregated state are obtained, resulting in a dual-channel intra/intermolecular exciplex (DCIE) emission with fast and efficient reverse intersystem crossing (RISC). Deep-blue OLED with Commission Internationale de l'Eclairage (CIE) coordinates of (0.157, 0.076) and a record-high external quantum efficiency (EQE) of 20.35% at high luminance (5000 cd m^{-2}) is accomplished. Simple molecular synthesis and device fabrication of this strategy give a unique approach to realizing high-performance deep-blue electroluminescence.

INTRODUCTION

As one of the most popular display and solid-state lighting solutions, organic light-emitting diodes (OLEDs) have attracted enormous attention and efforts to explore and accelerate their practical applications (*1*–*3*). In the current commercial products, phosphorescent emissive materials are used for green and red emissions thanks to their high efficiencies and stable device performances (*4*, *5*). However, because of the lack of suitable emitters, pure/deep-blue devices still rely on the first generation of purely fluorescent molecules with an internal quantum efficiency (IQE) below 25%, resulting in inferior device performances compared with its red and green counterparts (*6*–*9*). To solve this issue and meet the requirement of the National Television Standards Committee (NTSC) coordinates for "pure" blue of (0.14, 0.08) in commercial products, many efforts have been made by academia and industry all over the world. Similar to development strategies for green and red phosphorescent emitters, materials containing metal atoms (Ir, Pt, Au, Cu *et al.*) were designed and synthesized to obtain deep-blue emitters. Among them, the representative achievements were conducted by the group of Li (*10*), Forrest (*11*), Zysman-Colman (*12*), Credgington, and Thompson *et al.* (*13*, *14*). Some deep-blue phosphorescent OLEDs (PhOLEDs) with Commission Internationale de l'Eclairage *y* coordinates (CIE_y) of 0.05 to 0.11 and external quantum efficiencies (EQEs) of 11 to 24.8% have been accessed. Supposing the transport of electrons and holes can be more balanced, the stability of these phosphorescent emissive materials can be further improved, and the energy transmission and conversion efficiency can also be improved. In that case, it is possible to solve the problem of efficiency roll-off in PhOLEDs. In 2012, Ma and coworkers (*15*–*17*) proposed that hot exciton materials can convert the high triplet-state excitons (T_n, $n > 1$, hot excitons) to singlet-state ones (S_m, $m \geq 1$) through hybridized local and charge-transfer (HLCT) process, leading to 100% IQE. HLCT provides a strategy to obtain donor-π-acceptor type deep-blue molecules with low CIE_y, and the highest value of EQE can reach up to 10.8% with relatively low efficiency roll-off at present, which has great potential to obtain higher efficiency and stable deep-blue OLEDs.

Another important method to access deep-blue emission is the thermally activated delayed fluorescence (TADF) process. Adachi *et al.* achieved the breakthrough of TADF materials for OLEDs (*18*–*24*). In TADF molecules, the nonradiative triplet-state excitons (T_n, $n \geq 1$) can be upconverted to radiative S_1 excitons through reverse intersystem crossing (RISC), which is conducive to obtaining blue emission accompanied by 100% IQE in theory. The classic TADF molecules are based on the donor-acceptor (D-A) system. It has been proven that the intramolecular charge transfer (CT) via through-bond interaction effectively achieves good TADF emitters for OLEDs. For example, Kwon and Lee (*25*) reported that a deep-blue device based on a D-A molecule, TDBA–Ac, exhibited CIE coordinates of (0.15, 0.06) with a high EQE_{max} of 21.50 ± 0.22%. Besides the D-A type TADF molecules, Hatakeyama (*26*, *27*) designed and synthesized TADF molecules based on the multiple resonance (MR) effects of B and N atoms to achieve deep-blue OLED with $CIE_y < 0.1$ (0.09) and high EQE. Further study shows that deep-blue OLEDs based on MR-TADF could be constructed by using the MR effect of N/O and C/O atom pairs (*28*, *29*). Exciplex is a unique complex generated in situ through intramolecular or intermolecular charge transitions induced by light or electric fields (*30*–*33*). Holes on the highest occupied molecular orbital (HOMO) of the donor fragment and electrons on the lowest unoccupied molecular orbital (LUMO) of the acceptor motif are cross-recombined to form excitons and then emit light. Therefore, the exciplex strategy has the intrinsic potential to obtain the full color and TADF luminescence, including deep-blue emission, by independently adjusting the energy levels of the HOMO of the donor and LUMO of

[1]Key Laboratory of Advanced Display and System Applications, Ministry of Education, Shanghai University, 149 Yanchang Rd, 200072 Shanghai, China. [2]Institute of Organic Chemistry, Karlsruhe Institute of Technology (KIT), Fritz-Haber-Weg 6, 76131 Karlsruhe, Germany. [3]Institute of Biological and Chemical Systems-Functional Molecular Systems (IBCS-FMS), Karlsruhe Institute of Technology (KIT), Hermann-von-Helmholtz-Platz 1, D-76344 Eggenstein-Leopoldshafen, Germany.
*Corresponding author. Email: jhzhang@oa.shu.edu.cn (J.Z.); braese@kit.edu (S.B.); zxwang78@shu.edu.cn (Z.W.)
†These authors contributed equally to this work.

the acceptor. Currently reported representative intermolecular exciplexes connected by spiro- or oxygen bridge generally used acridines or diarylamines as donors, as reported by Jiang and Zhang, making the HOMO energy level of the molecule relatively shallow, which is conducive to achieving sky-blue luminescence (*34*, *35*).

To pursue ideal emitters for deep-blue OLEDs, we explored a novel material design strategy and synthesized the molecule **CzSiTrz** (Fig. 1). A silicon atom was used to connect the carbazole (Cz) and 1,3,5-triazine (Trz) moieties building a nonconjugated system. The efficient dual-channel intra/intermolecular exciplex (**DCIE**) TADF emission with fast RISC (k_{RISC} = 9.8 × 10^6 s^{-1}) is demonstrated. Using **CzSiTrz** as an emitter, deep-blue OLEDs with an emission peak at 440 nm, CIE coordinates of (0.157, 0.076), and record-high EQEs of 20.35% at high luminance (5000 cd m^{-2}) were realized.

RESULTS AND DISCUSSION

Molecule design and synthesis

We started our work on high-performance deep-blue OLEDs by designing and synthesizing the donor-Si-acceptor (D-Si-A) molecule, **CzSiTrz**. For comparison and emission property study purposes, the D-Si-D molecule, **CzSiCz**, and A-Si-A molecule, **TrzSiTrz**, were also synthesized (Fig. 1). The synthetic steps and characterization details are described in the Supplementary Materials. A carbazole donor was selected because of its planar structural geometry and deep HOMO energy level. In addition, the electron delocalization of planar Cz and Trz units enhances the electronic vibration coupling between them. At the same time, both Cz and Trz segments have high triplet energy levels of locally excited states (^{3}LE). After connecting these two components with silicon atoms, the first excited singlet state of charge transfer (^{1}CT) of CzSiTrz can be spin-orbit coupled well with their ^{3}LE, which can further enhance the RISC process (*36*).

Moreover, unlike the reported linking units, oxygen, hexafluoroisopropylidene, spirobifluorene bridge, etc., we use a silicon bridge as the central linking group to break the conjugation between donor and acceptor. The use of a Si bridge does not affect the electron cloud distribution of the donor and acceptor fragments, keeping them with a large energy gap for deep-blue emission. As reported by Sun and coworkers (*37*), the phenylsilyl group can stabilize the excited and polaronic states of the organic molecules through the hyperconjugation effect, which is favorable to producing efficient and stable intermolecular exciplex emission. In addition, the introduction of a silicon atom can play a positive role in improving the thermal performance of organic materials.

The glass transition temperature (T_g) and the thermal decomposition temperature (T_d) of **CzSiTrz** are 165° and 540°C, respectively (fig. S2 and Table 1). High T_g and T_d indicate that **CzSiTrz** can maintain good thermodynamic and morphological stability during the device manufacturing process.

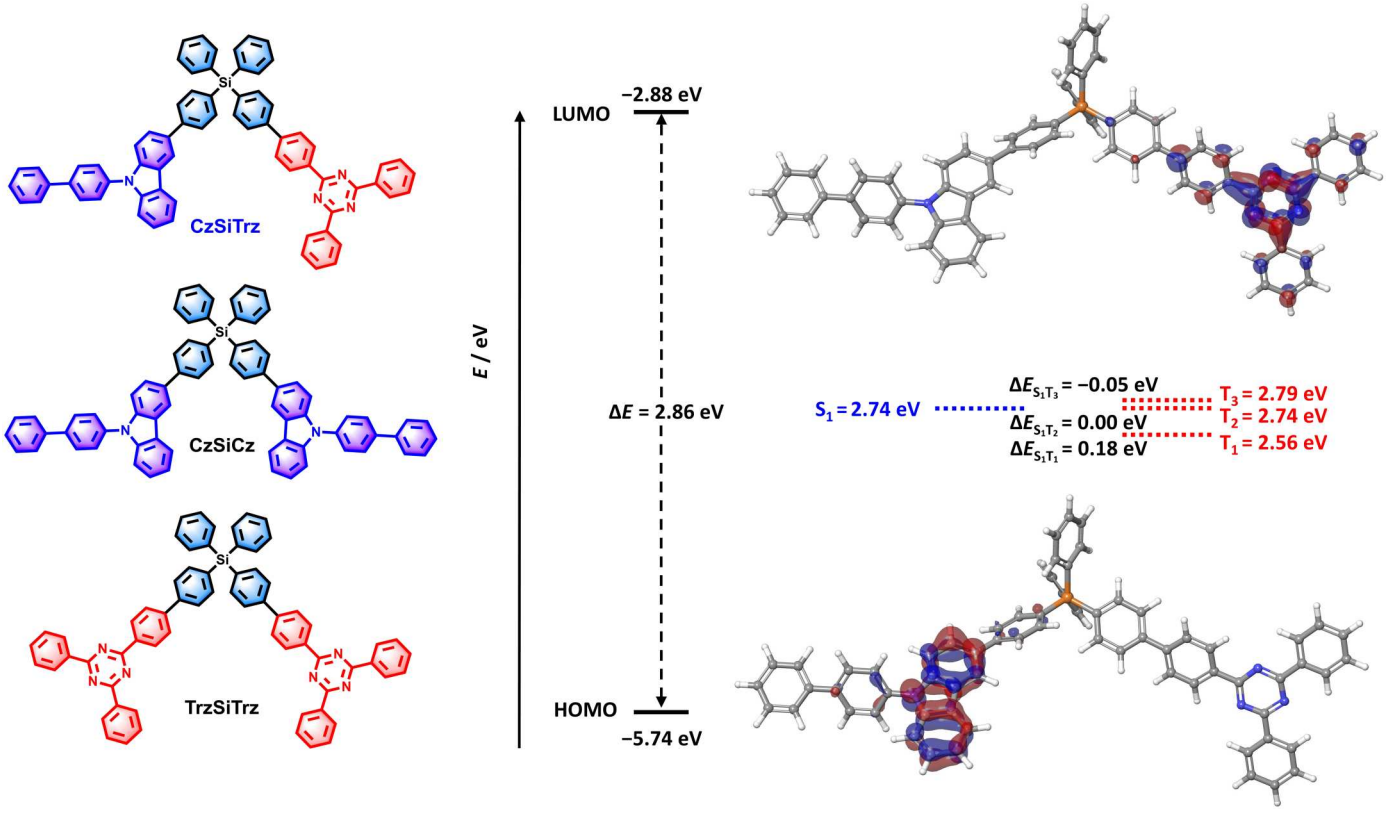

Fig. 1. Molecules and theoretical calculations. (Left) Chemical structures of **CzSiTrz**, **CzSiCz**, and **TrzSiTrz.** (Right) The optimized structure, frontier orbital densities (HOMO and LUMO), and energy states of **CzSiTrz**.

Table 1. Photophysical, electroluminescent, and thermal properties of CzSiTrz. DSC, differential scanning calorimetry.

Compound	λ_{PL}* (nm)	S_1/ T_1 (eV)	ΔE_{ST} (eV)	HOMO/ LUMO (eV)†	T_g/ T_d (°C)‡	PLQY (%)	τ_p (ns)	τ_d (μs)	k_{ISC} k_{RISC} ($\times 10^6$ s^{-1}) ($\times 10^6$ s^{-1})
CzSiTrz	377*/380§/ 445‖/448¶	3.12/ 3.06	0.06	5.62/2.88	165/540	83	35.5	0.11	2.6 9.8

*PL measured in cyclohexane. †The HOMO and LUMO values were determined using the following equations: HOMO (eV) = −(Eox + 4.8), LUMO (eV) = E_{HOMO} + Eg. The value of Eg was calculated from the absorption edges of films. ‡T_g, glass transition temperatures; T_d, thermal decomposition temperatures of 5% weight loss, obtained from DSC and TGA measurements. §PL measured in 0.1 wt % PMMA. ‖PL of neat **CzSiTrz** film at 298 K. ¶PL of neat **CzSiTrz** film at 77 K.

Theoretical calculations and electrochemical properties

Density functional theory (DFT) and time-dependent DFT calculations at the B3LYP/6-31G** level were carried out to reveal the electron cloud distributions and energy levels of **CzSiTrz**. The results are shown in Fig. 1 and Table 1. The HOMO is mainly located on the electron-donating carbazole fragment, and the LUMO is dispersed on the triazine moiety. The theoretically calculated HOMO and LUMO levels of **CzSiTrz** are −5.74 and −2.56 eV, respectively. Because of the nonconjugation effect of the Si atom, there is almost no overlap between HOMO and LUMO, resulting in a small ΔE_{S1T1} of 0.18 eV. In addition, it was found that the T_2 was identical to S_1 (2.74 eV), and the difference between T_3 and S_1 was also very small (ΔE_{S1T3} = −0.05 eV), which is conducive to realizing efficient RISC.

Cyclic voltammetry (CV) using the Fc^+/Fc redox pair as an internal standard was carried out to explore the electrochemical properties of **CzSiTrz** (fig. S3 and Table 1). As is typically observed for carbazole-based oxidations, **CzSiTrz** also showed an irreversible oxidation process with a potential peak at 0.82 eV. The reduction potential of −2.27 and −2.49 eV was observed, which could be assigned to the triazine unit. On the basis of these data, HOMO and LUMO levels were estimated at −5.62 and −2.88 eV, respectively.

Photophysical properties

The photoluminescent (PL) properties of **CzSiTrz** in solution were evaluated in different solvents first (Fig. 2A). It exhibited structured emission spectra with maximum emission peaks located at 359/377 nm in cyclohexane and 364/381 nm in toluene, which can be ascribed to the LE state transition of Cz or Trz units. PL emissions were also carried out in a dichloromethane (DCM) and 2-methyltetrahydrofuran (2-Me-THF) solution. As shown in Fig. 2A, besides emission peaks at 359 and 381 nm, another emission peak appeared at 506 nm (in 2-Me-THF) and 549 nm (in DCM) because of their higher polarities of them, which could be ascribed to the intramolecular through-space CT transition between Cz and Trz unit. Furthermore, the PL behaviors of **CzSiTrz** in mixed THF/water solvents were performed and analyzed (Fig. 2B). When water fraction (f_w) was below 30%, the fluorescence emission behavior was quite weak. The emission spectra were almost the same as in 2-Me-THF, with two emission ranges between 359 to 381 and 475 to 500 nm ascribed to the LE transition and intramolecular CT transition, respectively, between Cz or Trz units. When the f_w of water was increased to 50%, the emission intensity increased, and the emission at 484 nm became the stronger peak rather than that around 359 to 381 nm.

Further increasing the f_w of water, the longer emission became the dominant peak, and the intensity increased. However, when f_w is 90%, the strongest emission with a peak around 450 nm was obtained. In addition, the emission was blue-shifted with the f_w increase from 50% (482 nm) to 90% (450 nm). This could be ascribed to the reduction of Stokes shift, which may be derived from the crowded space and suppressed geometric relaxation. Therefore, **CzSiTrz** exhibited enhanced intensity and blue-shifted PL spectra peaks in the aggregation state. These results suggest that there are two channels of intramolecular and intermolecular CT emission processes to form their mixed luminescence when **CzSiTrz** gets aggregated to form nanoparticles as the distance between Cz and Trz units gets short. As a result, an efficient dual-channel intra/intermolecular exciplex (**DCIE**) emission was achieved.

To further confirm the **DCIE** features of **CzSiTrz** in neat film, PL emissions with different doping concentrations in polymethyl methacrylate (PMMA) film were performed and are shown in Fig. 2C. The PMMA films with 0.1 and 1% doping concentrations showed similar emission behaviors as in cyclohexane and toluene with LE transition emission and a tiny intramolecular CT emission. Notably, the PL spectrum of the film with 1 wt % doping concentration clearly exhibited a shoulder peak around 436 nm. **CzSiTrz** was doped into a nonpolar polymer, polystyrene, at a very low concentration (5×10^{-6} M); the emission bands between 400 and 460 nm were also observed after 40-ns decay (fig. S4) to verify the intramolecular CT emission too. As the doping concentration increases, the peaks between 350 and 385 nm become smaller and smaller, while the peaks at 436 nm become dominant. This suggests that there are strong LE state transitions and weak intramolecular CT transitions of **CzSiTrz** at lower doping concentrations, and strong intermolecular CT transitions dominate as the doping concentration increases while the molecules are relatively close aggregated. Ultimately, only an unstructured emission at 445 nm in the neat film was observed (Fig. 2C). Compared with the emission in solution with 90% f_w of water, the film emission shows almost the same shape and peak around 445 nm.

Moreover, as shown in Fig. 2D, the emission of **CzSiTrz** film at 445 nm is consistent with that of a 1:1 physical mixture of **CzSiCz** and **TrzSiTrz** (peak at 445 nm), which further confirmed the intermolecular interactions in nondoped **CzSiTrz** film. Therefore, the emission of the neat film should be attributed to **DCIE** transitions of **CzSiTrz** molecules. The PL emission of neat **CzSiTrz** film at 77 K was performed to explore its fluorescence and phosphorescence emission, and the excited singlet (^{1}CT) and triplet (^{3}CT) states were estimated at 3.12 and 3.06 eV on the basis of the onset of

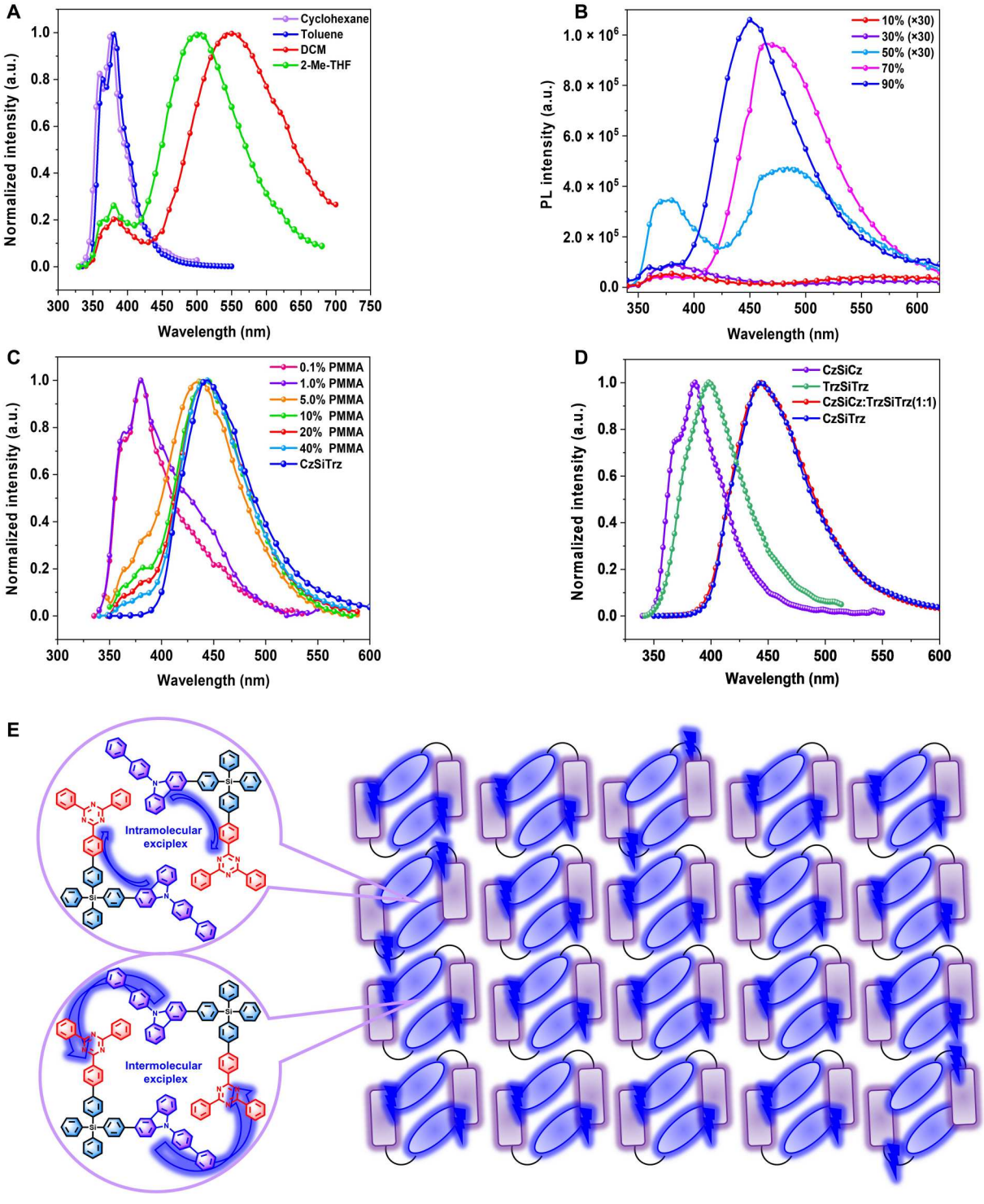

Fig. 2. Photophysical properties and molecular interactions. (**A**) PL spectra of **CzSiTrz** in solution. a.u., arbitrary units. (**B**) **CzSiTrz** in THF/water mixtures (10 μM) with water fraction (f_w) from 0 to 90% at room temperature. (**C**) **CzSiTrz** in PMMA with doped concentration from 0.1 to 100 wt % (neat film). (**D**) PL spectra of **CzSiTrz**, **CzSiCz**, **TrzSiTrz**, and **CzSiCz**:**TrzSiTrz** (1:1) film. (**E**) The possible processes of **DICE** in **CzSiTrz** film.

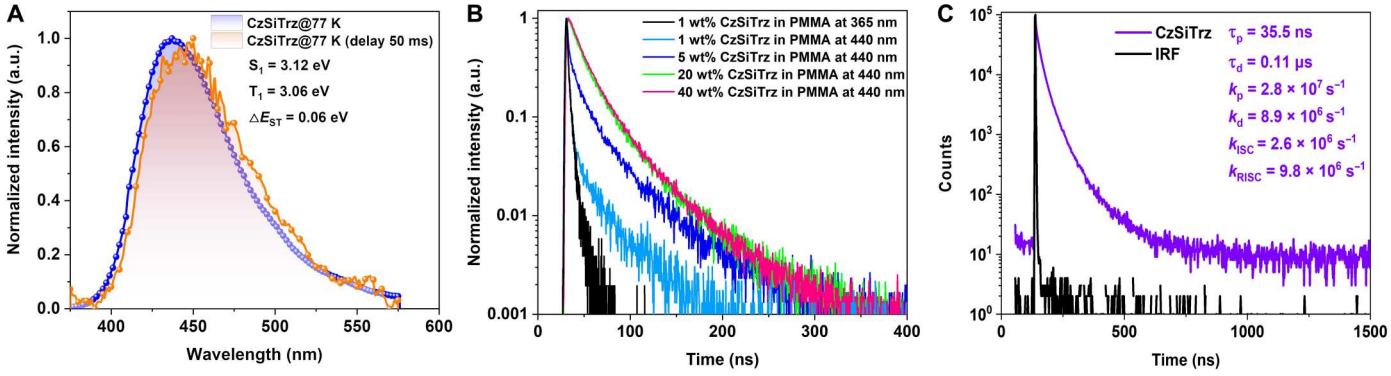

Fig. 3. Photophysical properties of CzSiTrz. (**A**) PL spectra of **CzSiTrz** neat film at room temperature and 77 K. (**B**) Transient PL decay spectra of **CzSiTrz** in PMMA. (**C**) Transient PL decay spectra of **CzSiTrz** neat film. The photoluminescent quantum yield (PLQY) in the PMMA matrix with a different doping concentration of **CzSiTrz** was performed. The results showed that PLQYs increased from 13% (0.1 wt %) to 43% (neat film). When the oxygen was excluded (under a nitrogen atmosphere), the PLQY was further increased to 83% (table S1). The transient decay of these PMMA films was explored to reveal the emission properties. The transient emission decay of 1 wt % **CzSiTrz** in PMMA film showed a delayed component at 436 nm from intramolecular CT emission, while it only showed the single exponential decay of ^{1}LE at 365 nm. As the doping concentration of **CzSiTrz** increased, the delayed component increased too. For the neat film, as shown in (C), the emission could be ascribed to the prompt fluorescence (PF) with a lifetime of 35.5 ns and the delayed fluorescence (DF) with a lifetime of 0.11 μs. On the basis of the lifetime and PLQY of **CzSiTrz** neat film, the rate of constant of PF (k_p) is calculated as 2.8×10^7 s^{-1}, which is higher than the rate of constant of DF (k_d) of 8.9×10^6 s^{-1}, because DF proceeds via a RISC of exciton from ^{3}CT to ^{1}CT and then returns to ground state. The intersystem crossing rate k_{ISC} is calculated to be 2.6×10^6 s^{-1}. Notably, the k_{RISC} of **CzSiTrz** is as fast as 9.8×10^6 s^{-1} based on the literature equation (S1.1 to S1.6 and fig. S6), which is one of the largest values of current reported results, including conventional D-A, unique MR, and intramolecular exciplex TADF molecules (table S2). Emission decays of neat film from 80 to 290 K (fig. S5) were measured and showed a temperature dependence typical for a TADF mechanism. The triplet states of the **Cz** donor and **Trz** acceptor segments are at 3.04 eV of ^{3}LE$_D$ and 3.01 eV of ^{3}LE$_A$, respectively (*36*). Because the connection of silicon atom completely breaks the conjugation between Cz and Trz, ^{3}LE$_D$ and ^{3}LE$_A$ are very close to the ^{1}CT and ^{3}CT of **CzSiTrz**, and the RISC process of ^{3}LE$_D$ or ^{3}LE$_A$ → ^{1}CT is easy to occur and dominates at low temperature resulting in large k_{RISC} value and little temperature dependence of decays (fig. S5). The large k_{RISC} indicates that the triplet state converting to the singlet state is very fast, and the exciton stays in the triplet state only for a very short time, which can suppress the exciton quenching. This confirms that **DCIE** is an efficient strategy for fast and efficient upconversion from T_1 to S_1, leading to an efficient TADF process.

spectra, respectively (Fig. 3A). As a result, a small ΔE_{ST} of 0.06 eV was accessed. This value is very small enough to activate a TADF process.

Electroluminescent properties

The deep-blue emission with a maximum peak at 445 nm and unique **DCIE** TADF features of **CzSiTrz** inspired us to explore its electroluminescent performances. Considering its aggregation-enhanced emission phenomenon, nondoped hole-only and electron-only device were fabricated first (fig. S8). It showed that **CzSiTrz** had better electron transport ability than hole transport ability. On the basis of these results, we fabricated nondoped OLED devices with the architecture of ITO/HATCN (10 nm)/NPB (15 nm)/TCTA (10 nm)/mCP (20 nm)/ **CzSiTrz** (X nm)/ASFT (Y nm)/ASFT:Liq (1:1) (20 nm)/Liq (1 nm)/Al (80 nm) (Fig. 4A). ITO (indium tin oxide) and Liq/Al were used as the anode, and the cathode, respectively; NPB (*N*,*N*′-di(naphthalen-1-yl)-*N*,*N*′diphenyl-benzidine) and TCTA (4,4′,4″-tris(carbazol-9-yl)triphenylamine) were used as the hole-transporting layers; 4-(3-(4,6-diphenyl-1,3,5-triazin-2-yl)phenyl)spiro[fluorene-9,5′-indeno[1,2-c]pyridine] (ASFT) was also used as the electron-transporting layer. 1,3-di(9H-carbazol-9-yl)benzene (mCP) was used as the exciton-blocking layer (Fig. 4A). The nondoped emissive layer was constructed using a neat **CzSiTrz** film.

Devices A, B, and C were fabricated with neat **CzSiTrz** of 5 nm and ASFT of 10, 15, and 20 nm, respectively. The turn-on voltages (V_{on}) of these devices were around 2.8 to 2.9 V (Table 2 and table S3), which is a new record for deep-blue OLEDs (emission peak <450 nm). The low voltages were due to using a nonconjugated connection mode that allowed to regulation of the injection of holes and electrons of molecules independently by D and A units. Their maximum EL emission peak was located at around 440 nm, which is consistent with their PL emissions. No other emission peaks were observed in devices A, B, and C, indicating that the emissions are only from **CzSiTrz** through the **DCIE** transition process. When ASFT was 15 nm (device B), maximum current efficiency (CE_{max}) of 17.3 cd A^{-1}, power efficiency (PE_{max}) of 16.8 lm W^{-1}, EQE_{max} of 21.5%, and CIE coordinates of (0.153, 0.079) were obtained. These performances were better than that of device A with ASFT of 10 nm because of more balanced charge transport. Moreover, the CIE coordinates of device B were very close to the standards of blue primaries (0.14, 0.08) of the NTSC. The high EQE_{max} of 21.5% is one of the best results for deep-blue OLEDs with peak emission <450 nm and CIE_y < 0.08. However, device B demonstrated a notable efficiency roll-off at a high luminance of 1000 cd m^{-2} (EQE = 17.6%, 18% roll-off) and 5000 cd m^{-2} (EQE = 8.5%, 60% roll-off). We further increased the ASFT to 20 nm in device C to enhance the electron transporting abilities. As a result, deep-blue device C with CIE coordinates of (0.157, 0.076) shows very stable efficiency performance, and its EQE gradually increases as the brightness increases. For a practical high luminance of 1000 cd m^{-2}, the EQE was 19.7%, comparable to the most efficient deep-blue OLEDs with maximum emission peak <450 nm and CIE_y < 0.08. The variation of CIE versus applied voltage is small, indicating that the emission spectra are relatively stable (fig. S9). To our best knowledge, the record-high EQE of 20.35% at 5000 cd m^{-2} and 20.43% at 7493 cd m^{-2} are the best performances at high luminance so far (Fig. 5 and table S3) (*38*–*43*). Its angular-resolved EL was

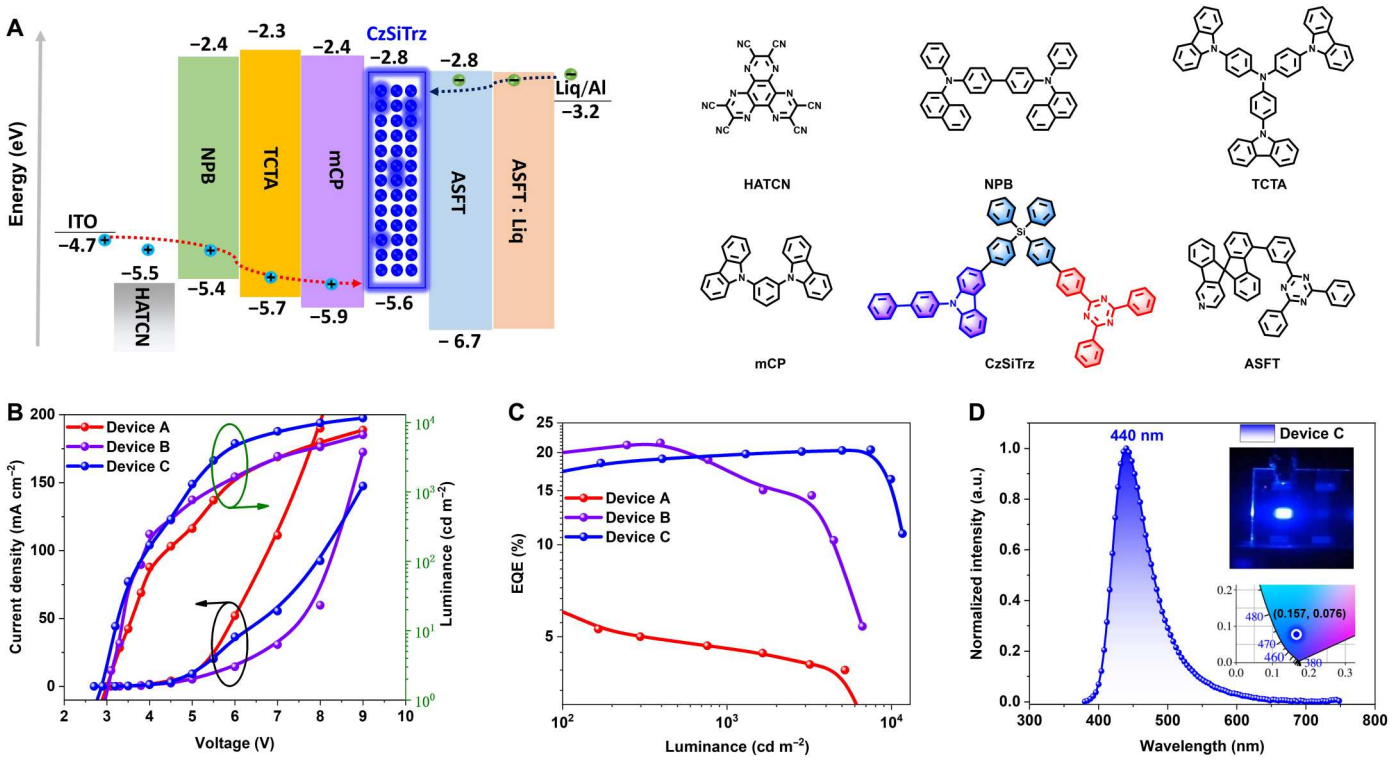

Fig. 4. Deep-blue devices based on CzSiTrz. (**A**) Device architecture and materials used in the devices A to E. (**B**) Current density–voltage–luminance characteristics (*J-V-L*) for devices A to C (*J-V* characteristics for device C from 0 to 9 V in fig. S12). (**C**) EQE versus luminescence curves for devices A to C. (**D**) EL spectra for devices C were obtained at 8 V.

measured and found to be very close to the standard Lambertian emission (fig. S10). In addition, the maximum luminance (L_{max}, 11,662 cd m^{-2}) of device C was also the best value of current reported deep-blue OLEDs with a maximum emission peak <450 nm, CIE_y < 0.08. The high luminance, EQE, and low-efficiency roll-off could be attributed to the **DCIE** TADF and the large k_{RISC} value (9.8 × 10^6 s^{-1}) through inhibiting the triplet-triplet and singlet-triplet exciton annihilation processes in the device. We also investigated the effect of **CzSiTrz** thickness on device performance. We constructed another nondoped device with the **CzSiTrz** thicknesses of 7 nm (device D, fig. S11). The maximum emission peak of device D is almost identical to device C, around 440 nm. The EQE_{max} of device D can reach up to 17.5%, lower than device C. Yet, it suffered from server efficiency roll-off at a high luminesce of 1000 cd m^{-2} (EQE = 16.1%, 8% roll-off) and 5000 cd m^{-2} (EQE = 9.0%, 66% roll-off for device D).

Notably, there is no very obvious difference in turn-on voltage of the four devices, which indicates that the charge injection is efficient and energy level differences between each functional layer are small too. The thickness of ASFT in device A is 10 nm; compared to many conventional OLED devices, device A showed the highest EQE at the lowest current density. With the increase in voltage, the current density also increases rapidly. Its EQE immediately decreases, and its efficiency roll-off is very obvious. With the increase of the thickness of ASFT, devices B, C, and D show a trend of EQE rising first with the increase of voltage and then roll-off. In these cases, the holes and electron pairs in the emitting layer are not balanced when applying voltage for the thicker ASFT, while, as the increase of voltage, the transmission of electrons increases rapidly, the holes and electron pairs in the emitting layer gradually tend to balance, and their EQEs reach the maximum value. Especially for device C, by adjusting the thickness of the hole and electron transport layers on both sides of the device, the carrier balance is further improved, resulting in a relatively high EQE at high luminance (5000 cd m^{-2}). As the voltage continues to increase, the holes and electrons are imbalanced again, resulting in the EQE decreasing with the brightness increase. Rapid aging at the same brightness is a conventional method to evaluate the lifetime of OLED devices. Devices with reduced efficiency roll-off usually have lower operating voltage and current density at high brightness, indicating that the hole and electron are well balanced in the emitting layer. Obviously, device C operated under lower voltage and current density is expected to have a long lifetime.

In this work, we connected substituted carbazole and 1,3,5-triazine as donor and acceptor, respectively, with nonconjugated Si atoms to construct a novel molecular system and obtained the representative molecule **CzSiTrz**. It is found that **CzSiTrz** forms intramolecular CT emission between D and A fragments by through-space exciplex. Strong intermolecular exciplex luminescence can also be formed in the solid state. Last, a **DCIE** emission with ultrafast RISC (k_{RISC} of 9.8 × 10^6 s^{-1}) was produced in its neat film because of efficient ^{3}CT-^{1}CT upconversion and spin-orbit coupling between $^3LE_{D,A}$ and ^{1}CT. On the basis of the strategy, deep-blue OLEDs with CIE_y < 0.08 and a record-high EQE over 20% at 5000 cd m^{-2} were demonstrated. Compared with the traditional D-π-A type TADF molecules, using nonconjugated silane to

Table 2. Electroluminescent device performances of deep-blue OLEDs based on CzSiTrz. FWHM, full width at half maximum.

Devices	V_{on} (V)	EL (nm)	Luminance (cd m^{-2})	CE/PE/EQE (cd A^{-1}/lm W^{-1}/%)			CIE(x,y)	FWHM (nm)
				Max	at 1000 cd m^{-2}	at 5000 cd m^{-2}		
A	2.9	444	7814	13.1/15.3/13.8	3.3/1.9/4.6	2.8/1.1/3.9	(0.153, 0.079)	59
B	2.9	444	6666	17.3/16.8/21.5	13.5/8.3/17.6	6.2/2.6/8.5	(0.154,0.079)	59
C	2.8	440	11662	14.1/ 12.0/20.43	14.0/9.1/19.7	13.7/7.2/20.35	(0.157,0.076)	58
D	3.1	444	6120	14.4/11.2/17.6	12.1/5.9/16.1	6.5/2.2/9.0	(0.155,0.081)	57

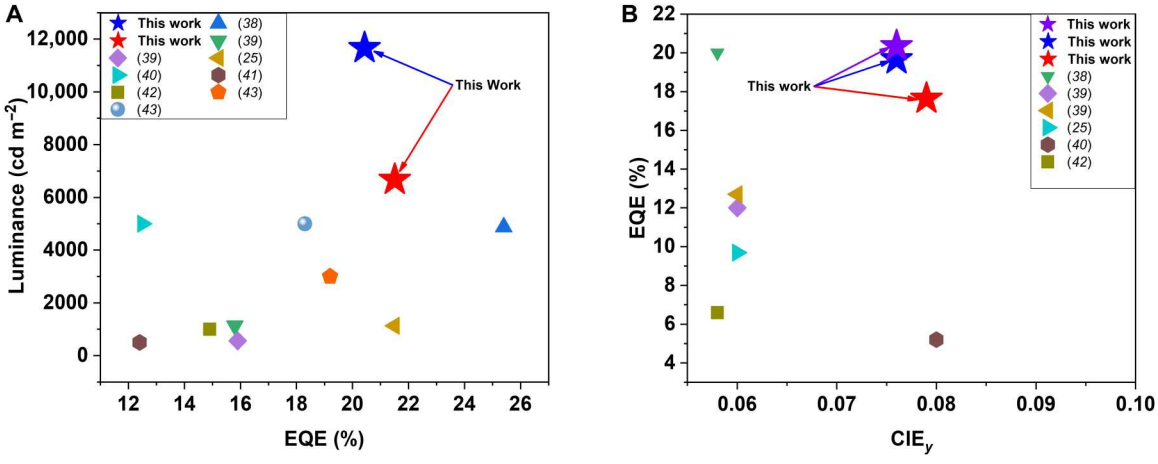

Fig. 5. Representative of purely organic emitters for deep-blue OLEDs with EL wavelength < 450 nm, CIE$_y$ < 0.10 (details in table S5). (**A**) EQE versus the maximum luminescence. (**B**) CIE$_y$ versus luminance at 1000 cd m^{-2} (the violet star, ★, for device C at 5000 cd m^{-2} in this work).

connect D and A segments with higher T_1 energy levels has obtained efficient deep-blue materials with good thermal stability. D and A groups are more abundant and various; this effective and unique design concept of chemical structure opens up an imaginary space for TADF materials with high k_{RISC}. It offers a promising method to achieve blue OLED devices with high performance in the future.

MATERIALS AND METHODS

All chemicals and reagents were used as received from commercial sources without further purification unless stated otherwise. The auxiliary materials for OLED fabrication were purchased from Yurui (Shanghai) Chemical Co. Ltd. ^{1}H nuclear magnetic resonance (NMR) and ^{13}C NMR spectra were recorded on a Bruker AV-500 spectrometer at room temperature. High-resolution mass spectra were determined on a Thermo Fisher Scientific LTQ FT Ultra mass spectrometer.

PL spectra were taken using an FLSP980 fluorescence spectrophotometer. The films on quartz substrate for photoluminescent quantum yield (PLQY) measurement were fabricated through vacuum thermal evaporation and encapsulated in the glovebox.

CV was carried out using a CH Instrument 660C electrochemical analyzer with an Ag/AgCl electrode as reference electrode, with tetra(*n*-butyl)ammonium hexafluorophosphate ($TBAPF_6$) in DMF as supporting electrolytes.

The glass transition temperature (T_g) of the compounds was determined under a nitrogen atmosphere by differential scanning calorimetry on a TA Q500 HiRes thermal analyzer using a scanning rate of 10°C/min with nitrogen flushing from 20° to 600°C. The decomposition temperature (T_d) corresponding to 5% weight loss was conducted on a TA Q500 HiRes TGA thermal analyzer.

All calculations in this study used Gauss 09 software. The molecular structures were optimized using the B3LYP algorithm 6-31G** basis set, and the HOMO and LUMO energy levels and the corresponding electron cloud distribution were calculated.

For OLED device fabrication, the organic layers were deposited consecutively on the precleaned ITO-coated glass substrates in vacuum conditions with a pressure of 8×10^{-5} Pa. The deposition rates of LiF, the organic materials, and aluminum were 0.6, 0.1, and 5 Å/s. The organic layers and the Al cathode were deposited without exposure to the atmosphere. The current density–voltage–luminescence (*J*-*V*-*L*) characteristics were measured by a Keithley 2400 source meter and a PR-670 Spectra Colorimeter in the direction perpendicular to the substrate at room temperature under ambient conditions.

Supplementary Materials

This PDF file includes:

Synthesis and Characterization
Supplementary Text
Figs. S1 to S20
Tables S1 to S3
References

REFERENCES AND NOTES

1. L. Xiao, Z. Chen, B. Qu, J. Luo, S. Kong, Q. Gong, J. Kido, Recent progresses on materials for electrophosphorescent organic light-emitting devices. *Adv. Mater.* **23**, 926–952 (2011).
2. J. Song, H. Lee, E. G. Jeong, K. C. Choi, S. Yoo, Organic light-emitting diodes: Pushing toward the limits and beyond. *Adv. Mater.* **32**, 1907539 (2020).
3. G. Hong, X. Gan, C. Leonhardt, Z. Zhang, J. Seibert, J. M. Busch, S. Bräse, A Brief history of OLEDs—Emitter development and industry milestones. *Adv. Mater.* **33**, 2005630 (2021).
4. X. Yang, G. Zhou, W.-Y. Wong, Functionalization of phosphorescent emitters and their host materials by main-group elements for phosphorescent organic light-emitting devices. *Chem. Soc. Rev.* **44**, 8484–8575 (2015).
5. H. Xu, R. Chen, Q. Sun, W. Lai, Q. Su, W. Huang, X. Liu, Recent progress in metal–Organic complexes for optoelectronic applications. *Chem. Soc. Rev.* **43**, 3259–3302 (2014).
6. X. Yang, X. Xu, G. Zhou, Recent advances of the emitters for high performance deep-blue organic light-emitting diodes. *J. Mater. Chem. C* **3**, 913–944 (2015).
7. Y. Im, S. Y. Byun, J. H. Kim, D. R. Lee, C. S. Oh, K. S. Yook, J. Y. Lee, Recent progress in high-efficiency blue-light-emitting materials for organic light-emitting diodes. *Adv. Funct. Mater.* **27**, 1603007 (2017).
8. T.-T. Bui, F. Goubard, M. Ibrahim-Ouali, D. Gigmes, F. Dumur, Thermally activated delayed fluorescence emitters for deep blue organic light emitting diodes: A review of recent advances. *Appl. Sci.* **8**, 494 (2018).
9. J. Tagare, S. Vaidyanathan, Recent development of phenanthroimidazole-based fluorophores for blue organic light-emitting diodes (OLEDs): An overview. *J. Mater. Chem. C* **6**, 10138–10173 (2018).
10. T. Fleetham, G. Li, L. Wen, J. Li, Efficient "Pure" Blue OLEDs employing tetradentate Pt complexes with a narrow spectral bandwidth. *Adv. Mater.* **26**, 7116–7121 (2014).
11. J. Lee, H.-F. Chen, T. Batagoda, C. Coburn, P. I. Djurovich, M. E. Thompson, S. R. Forrest, Deep blue phosphorescent organic light-emitting diodes with very high brightness and efficiency. *Nat. Mater.* **15**, 92–98 (2015).
12. A. K. Pal, S. Krotkus, M. Fontani, C. F. R. Mackenzie, D. B. Cordes, A. M. Z. Slawin, I. D. W. Samuel, E. Zysman-Colman, High-efficiency deep-blue-emitting organic light-emitting diodes based on Iridium(III) carbene complexes. *Adv. Mater.* **30**, 1804231 (2018).
13. D. Di, A. S. Romanov, L. Yang, J. M. Richter, J. P. H. Rivett, S. Jones, T. H. Thomas, M. A. Jalebi, R. H. Friend, M. Linnolahti, M. Bochmann, D. Credgington, High-performance light-emitting diodes based on carbene-metal-amides. *Science* **356**, 159–163 (2017).
14. R. Hamze, J. L. Peltier, D. Sylvinson, M. Jung, J. Cardenas, R. Haiges, M. Soleilhavoup, R. Jazzar, P. I. Djurovich, G. Bertrand, M. E. Thompson, Eliminating non-radiative decay in Cu(I) emitters: >99% quantum efficiency and microsecond lifetime. *Science* **363**, 601–606 (2019).
15. W. Li, D. Liu, F. Shen, D. Ma, Z. Wang, T. Feng, Y. Xu, B. Yang, Y. Ma, A twisting donor-acceptor molecule with an intercrossed excited state for highly efficient, deep-blue electroluminescence. *Adv. Funct. Mater.* **22**, 2797–2803 (2012).
16. H. Liu, Q. Bai, L. Yao, H. Zhang, H. Xu, S. Zhang, W. Li, Y. Gao, J. Li, P. Lu, H. Wang, B. Yang, Y. Ma, Highly efficient near ultraviolet organic light-emitting diode based on a meta-linked donor–Acceptor molecule. *Chem. Sci.* **6**, 3797–3804 (2015).
17. Y. Xu, P. Xu, D. Hu, Y. Ma, Recent progress in hot exciton materials for organic light-emitting diodes. *Chem. Soc. Rev.* **50**, 1030–1069 (2021).
18. H. Uoyama, K. Goushi, K. Shizu, H. Nomura, C. Adachi, Highly efficient organic light-emitting diodes from delayed fluorescence. *Nature* **492**, 234–238 (2012).
19. Q. Zhang, B. Li, S. Huang, H. Nomura, H. Tanaka, C. Adachi, Efficient blue organic light-emitting diodes employing thermally activated delayed fluorescence. *Nat. Photonics* **8**, 326–332 (2014).
20. S. Hirata, Y. Sakai, K. Masui, H. Tanaka, S. Y. Lee, H. Nomura, N. Nakamura, M. Yasumatsu, H. Nakanotani, Q. Zhang, K. Shizu, H. Miyazaki, C. Adachi, Highly efficient blue electroluminescence based on thermally activated delayed fluorescence. *Nat. Mater.* **14**, 330–336 (2014).
21. M. Y. Wong, E. Zysman-Colman, Purely organic thermally activated delayed fluorescence materials for organic light-emitting diodes. *Adv. Mater.* **29**, 1605444 (2017).
22. Z. Yang, Z. Mao, Z. Xie, Y. Zhang, S. Liu, J. Zhao, J. Xu, Z. Chi, M. P. Aldred, Recent advances in organic thermally activated delayed fluorescence materials. *Chem. Soc. Rev.* **46**, 915–1016 (2017).
23. Y. Liu, C. Li, Z. Ren, S. Yan, M. R. Bryce, All-organic thermally activated delayed fluorescence materials for organic light-emitting diodes. *Nat. Rev. Mater.* **3**, 18020 (2018).
24. Y. Fu, H. Liu, D. Yang, D. Ma, Z. Zhao, B. Z. Tang, Boosting external quantum efficiency to 38.6% of sky-blue delayed fluorescence molecules by optimizing horizontal dipole orientation. *Sci. Adv.* **7**, eabj2504 (2021).
25. D. H. Ahn, S. W. Kim, H. Lee, I. J. Ko, D. Karthik, J. Y. Lee, J. H. Kwon, Highly efficient blue thermally activated delayed fluorescence emitters based on symmetrical and rigid oxygen-bridged boron acceptors. *Nat. Photonics* **13**, 540–546 (2019).
26. T. Hatakeyama, K. Shiren, K. Nakajima, S. Nomura, S. Nakatsuka, K. Kinoshita, J. Ni, Y. Ono, T. Ikuta, Ultrapure blue thermally activated delayed fluorescence molecules: Efficient HOMO-LUMO separation by the multiple resonance effect. *Adv. Mater.* **28**, 2777–2781 (2016).
27. Y. Kondo, K. Yoshiura, S. Kitera, H. Nishi, S. Oda, H. Gotoh, Y. Sasada, M. Yanai, T. Hatakeyama, Narrowband deep-blue organic light-emitting diode featuring an organoboron-based emitter. *Nat. Photonics* **13**, 678–682 (2019).
28. Y. Yuan, X. Tang, X. Y. Du, Y. Hu, Y. J. Yu, Z. Q. Jiang, L. S. Liao, S. T. Lee, The design of fused amine/carbonyl system for efficient thermally activated delayed fluorescence: Novel multiple resonance core and electron acceptor. *Adv. Opt. Mater.* **7**, 1801536 (2019).
29. D. Hall, S. M. Suresh, P. L. dos Santos, E. Duda, S. Bagnich, A. Pershin, P. Rajamalli, D. B. Cordes, A. M. Z. Slawin, D. Beljonne, A. Köhler, I. D. W. Samuel, Y. Olivier, E. Zysman-Colman, Improving processability and efficiency of resonant TADF emitters: A design strategy. *Adv. Opt. Mater.* **8**, 1901627 (2019).
30. Q. Wang, Q.-S. Tian, Y.-L. Zhang, X. Tang, L.-S. Liao, High-efficiency organic light-emitting diodes with exciplex hosts. *J. Mater. Chem. C* **7**, 11329–11360 (2019).
31. M. Zhang, C.-J. Zheng, H. Lin, S.-L. Tao, Thermally activated delayed fluorescence exciplex emitters for high-performance organic light-emitting diodes. *Mater. Horiz.* **8**, 401–425 (2021).
32. Q. Xue, G. Xie, Thermally activated delayed fluorescence beyond through-bond charge transfer for high-performance OLEDs. *Adv. Opt. Mater.* **9**, 2002204 (2021).
33. Y. Wang, J. H. Yun, L. Wang, J. Y. Lee, High triplet energy hosts for blue organic light-emitting diodes. *Adv. Funct. Mater.* **31**, 2008332 (2020).
34. X. Tang, L.-S. Cui, H.-C. Li, A. J. Gillett, F. Auras, Y.-K. Qu, C. Zhong, S. T. E. Jones, Z.-Q. Jiang, R. H. Friend, L.-S. Liao, Highly efficient luminescence from space-confined charge-transfer emitters. *Nat. Mater.* **19**, 1332–1338 (2020).
35. Y.-Z. Shi, K. Wang, X. Li, G.-L. Dai, W. Liu, K. Ke, M. Zhang, S.-L. Tao, C.-J. Zheng, X.-M. Ou, X.-H. Zhang, Intermolecular charge-transfer transition emitter showing thermally activated delayed fluorescence for efficient non-doped OLEDs. *Angew. Chem. Int. Ed.* **57**, 9480–9484 (2018).
36. T. Wang, A. K. Gupta, S. Wu, A. M. Z. Slawin, E. Zysman-Colman, Conjugation-modulated excitonic coupling brightens multiple triplet excited states. *J. Am. Chem. Soc.* **145**, 1945–1954 (2023).
37. J. Sun, H. Ahn, S. Kang, S.-B. Ko, D. Song, H. A. Um, S. Kim, Y. Lee, P. Jeon, S.-H. Hwang, Y. You, C. Chu, S. Kim, Exceptionally stable blue phosphorescent organic light-emitting diodes. *Nat. Photonics* ***16***, 212–218 (2022).
38. G. Xia, C. Qu, Y. Zhu, J. Ye, K. Ye, Z. Zhang, Y. Wang, A TADF emitter featuring linearly arranged spiro-donor and spiro-acceptor groups: Efficient nondoped and doped deep-blue OLEDs with CIE_y < 0.1. *Angew. Chem. Int. Ed.* **60**, 9598–9603 (2021).
39. H. J. Kim, H. Kang, J. E. Jeong, S. H. Park, C. W. Koh, C. W. Kim, H. Y. Woo, M. J. Cho, S. Park, D. H. Choi, Ultra-deep-blue aggregation-induced delayed fluorescence emitters: Achieving nearly 16% EQE in solution-processed nondoped and doped OLEDs with CIE_y < 0.1. *Adv. Funct. Mater.* **31**, 2102588 (2021).
40. D. H. Ahn, H. Lee, S. W. Kim, D. Karthik, J. Lee, H. Jeong, J. Y. Lee, J. H. Kwon, Highly twisted donor–Acceptor boron emitter and high triplet host material for highly efficient blue thermally activated delayed fluorescent device. *ACS Appl. Mater. Interfaces* **11**, 14909–14916 (2019).
41. Y. Im, S. H. Han, J. Y. Lee, Deep blue thermally activated delayed fluorescent emitters using CN-modified indolocarbazole as an acceptor and carbazole-derived donors. *J. Mater. Chem. C* **6**, 5012–5017 (2018).
42. Y. H. Lee, S. Park, J. Oh, S.-J. Woo, A. Kumar, J.-J. Kim, J. Jung, S. Yoo, M. H. Lee, High-efficiency sky blue to ultradeep blue thermally activated delayed fluorescent diodes based on *ortho*-carbazole-appended triarylboron emitters: Above 32% external quantum efficiency in blue devices. *Adv.Opt. Mater.* **6**, 1800385 (2018).
43. L. S. Cui, H. Nomura, Y. Geng, J. U. Kim, H. Nakanotani, C. Adachi, Controlling singlet–Triplet energy splitting for deep-blue thermally activated delayed fluorescence emitters. *Angew. Chem. Int. Ed.* **56**, 1571–1575 (2017).

44. Y. Tsuchiya, S. Diesing, F. Bencheikh, Y. Wada, P. L. dos Santos, H. Kaji, E. Zysman-Colman, I. D. W. Samuel, C. Adachi, Exact solution of kinetic analysis for thermally activated delayed fluorescence materials. *J. Phys. Chem. A* ***125***, 8074–8089 (2021).

Acknowledgments

Funding: This work is financially supported by the State's Key Project of Research and Development Plan (no. 2022YFE0109000), the National Science Fund of China (nos. 51725505 and 21975152), and the China Postdoctoral Science Foundation (no. 2022 M722028). This research is also funded by the Deutsche Forschungsgemeinschaft (DFG, German Research Foundation) under Germany's Excellence Strategy via the Excellence Cluster 3D Matter Made to Order (EXC-2082/1–390761711) and the KIT-Publication Fund of the Karlsruhe Institute of Technology. **Author contributions:** Conceptualization: Z.Z., S.B., and Z.W. Methodology: Z.Z., D.D., R.X., K.W., E.S., J.C., S.B., and Z.W. Investigation: Z.Z., D.D., R.X., and P.W. Visualization: Z.Z., D.D., R.X., and P.W. Funding acquisition: J.Z. and Z.W. Project administration: Z.Z., Z.W., B.W., X.L., and J.Z. Supervision: S.B. and Z.W. Writing—original draft: Z.Z. and Z.W. Writing—review and editing: Z.Z., E.S., S.B., and Z.W. **Competing interests:** The authors declare that they have no competing interests. **Data and materials availability:** All data needed to evaluate the conclusions in the paper are present in the paper and/or the Supplementary Materials.

Submitted 19 October 2022
Accepted 18 April 2023
Published 19 May 2023
10.1126/sciadv.adf4060

ScienceAdvances

Efficient deep-blue luminescence based on dual-channel intra/intermolecular exciplexes

Zhen Zhang, Dehai Dou, Rongrong Xia, Peng Wu, Eduard Spuling, Ke Wang, Jin Cao, Bin Wei, Xifeng Li, Jianhua Zhang, Stefan Brse, and Zixing Wang

Sci. Adv., **9** (20), eadf4060.
DOI: 10.1126/sciadv.adf4060

Science Advances (ISSN) is published by the American Association for the Advancement of Science. 1200 New York Avenue NW, Washington, DC 20005. The title *Science Advances* is a registered trademark of AAAS.